International Journal of Electrical, Electronic and Communication Sciences
ISSN: 2517-9438
Vol:12, No:4, 2018

Numerical and Experimental Assessment of a PCM Integrated Solar Chimney

J. Carlos Frutos Dordelly, M. Coillot, M. El Mankibi, R. Enríquez Miranda, M. José Jimenez, J. Arce Landa

***Abstract*—**Natural ventilation systems have increasingly been the subject of research due to rising energetic consumption within the building sector and increased environmental awareness. In the last two decades, the mounting concern of greenhouse gas emissions and the need for an efficient passive ventilation system have driven the development of new alternative passive technologies such as ventilated facades, trombe walls or solar chimneys. The objective of the study is the assessment of PCM panels in an in situ solar chimney for the establishment of a numerical model. The PCM integrated solar chimney shows slight performance improvement in terms of mass flow rate and external temperature and outlet temperature difference. An increase of 11.3659 m^3/h can be observed during low wind speed periods. Additionally, the surface temperature across the chimney goes beyond 45 °C and allows the activation of PCM panels.

***Keywords*—**Energy storage, passive ventilation, phase changing materials, solar chimney, solar energy.

I. Introduction

A solar chimney (SC) is a technology that has existed for centuries, particularly useful in hot climates. SC designs are a modified version of wind towers employed in Persian architecture. In its simplest form, it is an air channel employed to evacuate hot air to the exterior through the buoyancy effect. The materials employed for its construction can vary depending on the design. Most modern studies of SC analyse variables such as the aspect ratio between inlet and outlet, height, inclination or air gap width; however, few focus on prolonging air circulation in the absence of a heat source through the implementation of energy storage. An Active Solar Chimney (ASC) employs energy storage devices to improve the performance of the current SC.

A. Literature Review

The pioneering work of Bansal et al. [1] introduced the advantages of SC through the development of a steady state mathematical model which analyzed the mass flow rate for different size openings. It was stated that it is possible to induce an airflow of 100 - 350 m^3/h; however, the efficiency of the chimney depends on the geometry of the collector wall, the cross-section of the duct and the characteristics of the collector.

AboulNaga and Abdrabboh [2] determined that the SC could be employed for nocturnal ventilation. They carried out a predictive theoretical study of the effects of a wall-roof inclined solar chimney (WRISC) for different chimney sizes and inlet heights. It is stablished that in arid countries such as the UAE, the cooling load of a residential building could be decreased by 24% with such building component.

Other authors such as Khanal et al. [3] (and their previous works) address the advantages of SC as an alternative solution for ventilation in terms of operational cost, energy requirement and CO_2 emissions. Their research focuses on the improvement of the ventilation performance through two main aspects of the SC: the effect of the geometry, and the effect of tilt angle. Their work, based on the Inclined Passive Wall Solar Chimney (IPWSC), mentions the possibility of passive heating and cooling through the implementation of a SC for the reduction of HVAC loads. The main focus of their studies was the determination of flow scenarios occurring during natural ventilation in an IPWSC, in terms of the Rayleigh number, concluding that a tilt angle can improve by 17% the mass flow rate for high Rayleigh numbers, and it counteracts reverse flow problems.

Chen et al. [4] carried out an analytical and experimental research in order to find the ideal gap-to-height ratio, for an inclined SC. Their findings state the best mass flow rate results for a 200 mm gap and 1.5 m tall chimney were obtained at a 45° inclination with no apparent optimum chimney gap, nonetheless, it is stated that for a fixed inlet size, the increase of the air gap can lead to the decrease of mass flow rate. Results show that an inclination of 45° and 60°can improve airflow in 45% and 30% respectively. This improvement is described as the result of both increased stack pressure and reduced pressure losses across the chimney.

In addition, studies such as the one carried out by Liu et al. [5] suggest that the even though no optimum air gap width has been established, a gap-to-height ratio of 0.2 to 0.3 yields the better mass flow rate results.

Other researches have analysed the contribution of mechanical components for hybrid ventilation [6]; however, even though it was stated that mechanical ventilation can increase the ventilation rate, it was demonstrated that it could lead to reverse flow scenarios, for high mechanical ventilation volumes due to the greater inflow pressure. Moreover, it has been stated [7] that almost 2/3 of the incoming solar energy is

J. C. Frutos Dordelly is with the Ecole Nationale des Travaux Publics de l'Etat, Vaulx-en-Velin 69518, France (phone: +33 4 72 04 72 47; e-mail: carlos.frutosdordelly@entpe.fr).

M. Coillot and M. El Mankibi are with the Ecole Nationale des Travaux Publics de l'Etat, Vaulx-en-Velin 69518, France (e-mail: mike.coillot@entpe.fr, mohamed.elmankibi@entpe.fr).

R. Enríquez Miranda and M. J. Jimenez are with the Centro de Investigaciones Energéticas, Medioambientales y Tecnológicas, Madrid 28040, Spain (e-mail: ricardo.enriquez@ciemat.es, jesuso@cenidet.edu.mx).

is with the Centro de Investigaciones Energéticas, Medioambientales y Tecnológicas, Tabernas 04200, Spain (e-mail: Maria Jose Jimenez (mjose.jimenez@psa.es).

lost at or through the glass cover, which suggests the need for additional optimization and the pursuit of enhanced thermal inertia within the chimney over a mechanical solution.

In literature, SC have been coupled to building walls (wall-roof SC), trombe walls or windows [2], [8], however; these solutions aim to improve the performance of the chimney when in presence of an energy source. Naraghi et al. [9] demonstrated that, by increasing the thermal mass of the absorber plate, the mass flow rate during the evening and the early morning is as well enhanced, thus improving the utility of SC.

B. Objectives and Methodology

The main objective of the article is to compare the implementation of energy storage devices - mainly paraffinic RT44 phase changing material (PCM) panels - assessed under laboratory and *in situ* conditions against a numerical model developed with MATLAB/Simulink. The in-situ experimentation is a collaboration with the CIEMAT in Tabernas, Spain and a continuation of the work done by Arce et al. [10]

A preliminary study [11] on an individual panel was carried out to characterise the behaviour of the paraffinic material, macroencapsulated in the aluminium panels. The feasibility of RT44 panels was compared through laboratory and in-situ experiments, analysed through an experimental protocol recording temperature and airflow evolution across the SC prototype. Surface temperatures were recorded at different heights during the study to observe the temperature evolution between inlet and outlet. Tests were carried out with and without RT44 panels to evidence the difference between a classic SC and the ASC.

Preliminary results produced by the individual panel display the behaviour of the material and exhibit the capacity for energy storage along with the change of phase. Initial results show a clear temperature difference for three different heights across the laboratory SC prototype (1 m, 2.5 m, and 4 m). Indeed, the results for the prototype without PCM register an important temperature difference (approximately 15 °C) between the lower and the higher surface temperature sensors. Furthermore, ASC results demonstrate a more even temperature distribution across the different heights. Moreover, outlet airflow results reveal the impact of PCM panels for a prolonged use.

PCM panels were implemented because of their capacity to release stored energy and create thermal inertia. The performance of these materials is highly dependent on the incoming energy, therefore further studies are required to ensure the complete change of state. Initial tests show an increase in the outlet air flow of the prototype in absence of a heating source. These findings were compared to the in-situ experiment to observe the influence of external factors (e.g. wind speed, humidity) on the performance of the system. The robustness of the numerical model was assessed against these results.

II. Experimental Setup

A. Solar Chimney

The stand-alone chimney depicted in Fig. 1 was developed in Tabernas, Spain in 2009 at the "Plataforma Solar de Almeria" (PSA). The latest iteration of the system is 5.60 m tall, 1.20 m width and 0.52 m deep. The chimney is composed of a 0.15-m thick concrete absorbing plate, thermal insulation behind the concrete plate, a 5-mm thick glass cover to reduce convective and radiative losses to the environment, a wood casing, and a driving air protection, which generates a fall of pressure near the exit, and at the same, time aids the extraction of air. The prototype is shown in Fig. 1.

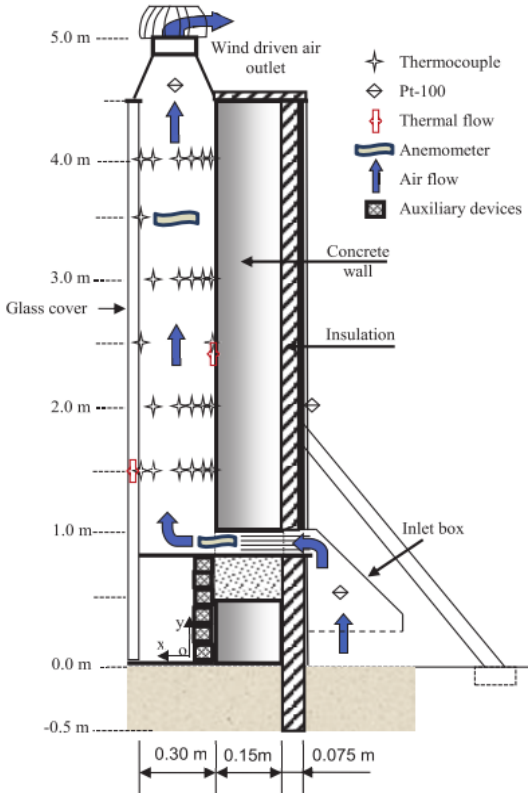

Fig. 1 Lateral view of the SC and the instrumentation set up built by Arce et al. [10]

B. Active SC

In order to assess the implementation of PCMs on the aforementioned SC, 21 panels were distributed over the surface of the prototype as shown in Fig. 2. Sensors were placed in seven panels at three different levels: inlet level at 1m, mid-level at 3 m and outlet level at 4 m. These sensors were added to the free channels of the existing acquisition modules in order to maintain the coherence of the signals.

III. Instrumentation

The experimental instrumentation used for the different measurements of the SC is detailed in the technical note published by Arce et al. [12]. Platinum thermoresistance

(PT100, 1/10 DIN) sensors are used to record surface temperature of the panels via a four-wire connection. These sensors consist of a very small sensing element embedded in a slim rubber substrate. The sensors were glued to the centre of the panels as marked in Fig. 2 and painted black matte to integrate them as much as possible with the corresponding surface.

A data acquisition system with the following characteristics is being used: 16-bit A/D resolution, range of measurements fitting sensor output, modules distributed to minimize wiring, based in Compact Field Point modules manufactured by NATIONAL INSTRUMENTS.

The PSA counts with its own meteorological station, which measures data ever second. Data are averaged and recorded every minute. Further details concerning the meteorological station can be found in the aforementioned article.

IV. Numerical Model

The numerical model is composed of two separate systems, coupled through a MATLAB/Simulink R2017b interface: firstly, a heat transfer model of a multi-layered wall containing the temperature dependent properties of a PCM layer followed by the aerodynamic model that analyzes the air temperature, speed, and pressure distribution.

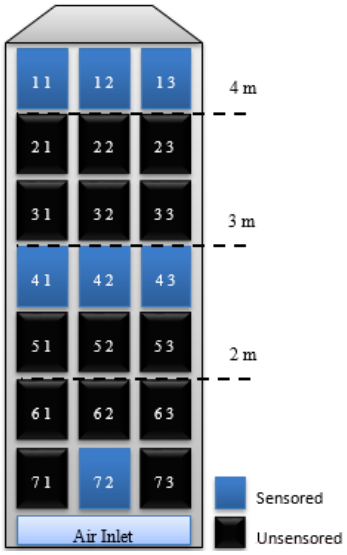

Fig. 2 Panel distribution and sensor placement on the PSA SC

A. Heat Transfer through a Multilayered Wall

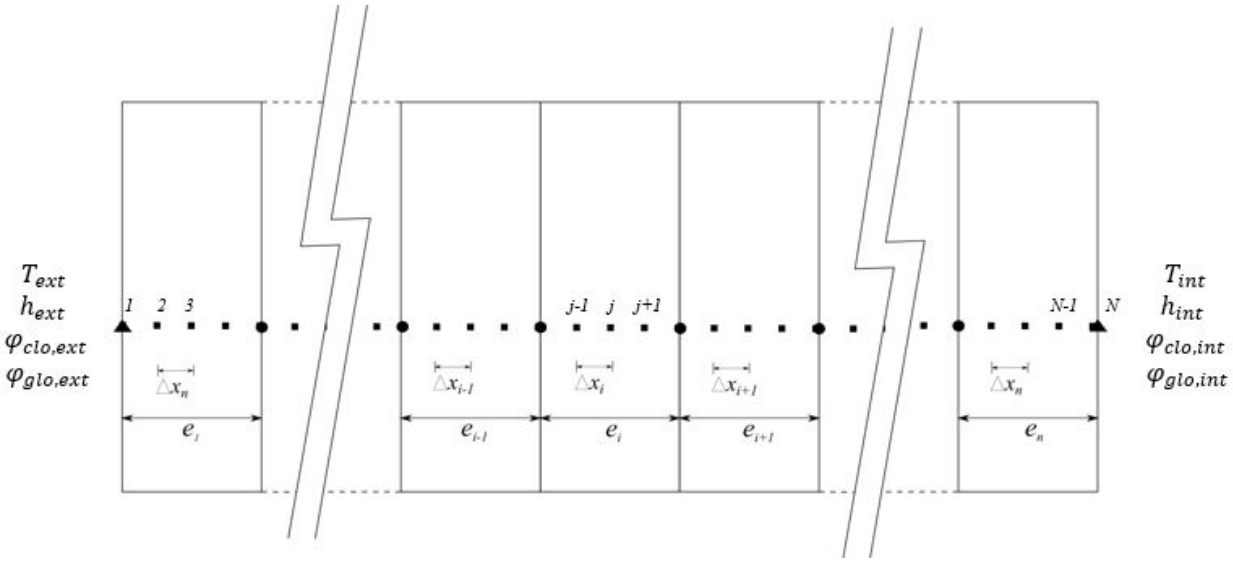

Fig. 3 Spatial discretization of a *n* layer multilayered wall

The model was developed using a finite-difference Crank-Nicholson implicit method, which follows a central difference scheme at time $t_{n+1/2}$ and a second order central difference for the space derivative at position x_i by setting the new variable $\bar{T}$.

$$\bar{T}_i = \frac{T_i^{t+\Delta t} + T_i^t}{2} \quad (1)$$

A more detailed explanation of the multilayered wall numerical model can be found in the previous work [11].

B. PCM Integration in a Multilayered Wall

In order to account for the non-linear behavior of phase changing materials, several options were considered. Some studies have explained the behavior of phase changing materials by setting three different working phases: solid, liquid and transitory state [13]. Studies such as the one carried out by Mirzaei and Haghighat [14] have modelled the behavior in similar ways, adding a discretization along the PCM layer to simulate the progressive phase change of the

material. Other articles have opted to work on different approaches such as DTA (Differential thermal analysis) [15] and DSC (Differential scanning calorimetry) tests [16], both techniques in which the difference in the amount of heat required to increase the temperature of a sample and reference is measured as a function of temperature. This last technique was chosen over other options since the data from the test can be simply input into the code instead of calculated at each time interval, thus reducing the calculation time of the numerical model.

The results of the DSC test for the Rubitherm RT44 phase changing material are shown in Fig. 4. This test was carried out at a cooling/heating speed of 0.05 °C/min, according to the expected charge/discharge speed of the panels in the chimney. The specific heat of the RT44 material is input to each node of the discretization as a function of temperature $C_p(T)$, allowing a more specific evolution along the PCM layer. Specific heat is calculated using the following expression:

$$C_p(T) = \frac{DSC(T)_S}{\varphi} \quad (2)$$

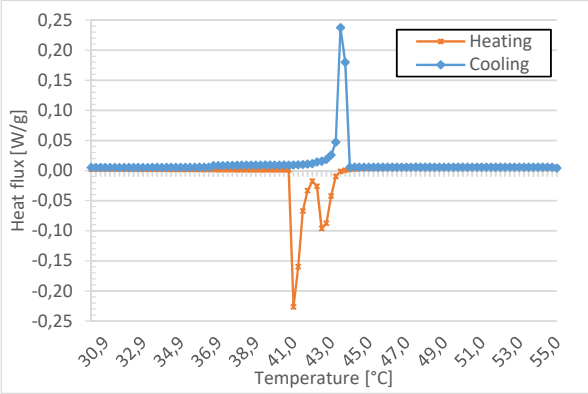

Fig. 4 DSC results for the RT44 phase changing material showing the evolution of heat flux as function of temperature

C. Radiation Model

Only diffuse and opaque gray bodies are considered except for the transparent glazing. The main exchanges are those with short and long wavelengths. The surface conditions are treated in the same manner. Short wavelengths are considered as belonging to the visible range between 380 and 780 nm. They are characteristic of radiative exchanges involving solar inputs. GLO (Long wavelength) exchanges are considered to be characteristic of low-temperature exchanges between the walls of the DF. This concerns wavelengths greater than 780 nm.

The objective is to obtain, with the help of the wall temperatures and solar gains, the net flux of each surface. It is equal to the difference between the flow emitted and the flow absorbed. The model is based on the calculation of the incident CLO (short wavelength) and GLO radiations. The calculation is then coupled with the multilayered wall code.

$$\phi_{net} = \phi_{emitted} - \phi_{absrobed} \quad (3)$$

$$\phi_{emitted} = \epsilon\sigma T^4 \quad (4)$$

$$\phi_{absrobed} = \alpha_{GLO}E_{GLO} - \alpha_{CLO}E_{CLO} \quad (5)$$

where ϵ is the emissivity of the surface, α the absorptance, σ the Stefan-Boltzmann constant and E the incident radiation of long and short wavelengths.

D. Pressure Code – A Zonal Approach

In order to assess and compare the performance of the SC against the ASC, an aerodynamic model was developed for the calculation of pressures across the volume discretization of the chimney. In turn, this information was employed for the determination of the mass flow rate, a key variable for the evaluation of the chimney performance along with the conduit temperature.

As stated before, the chimney was divided into seven control volumes (along the length of the chimney) according to the dimensions of the chimney and the size of the PCM panels: $1 \times 0.3 \times 0.5\ m$. Each volume must solve the mass balance equation for a given pressure and a defined temperature. The results are subsequently communicated to neighbouring volumes for several iterations until the system arrives to a solution at each time step. The model iterates until the pressure values attain a convergence factor of $1x10^{-6}$.

$$\sum_{k=1}^{j} \dot{m}_{ik} = 0 \quad (6)$$

The mass flow rate depends on the pressures of the neighbouring cells. The mass exchange between common interfaces will serve to calculate the new pressure distribution through several iterations. Density fluctuates due to temperature differences between adjacent zones, which leads to buoyancy driven flow. The pressure zonal approach uses the information obtained through the heat transfer model to establish and recalculate the temperature distribution across the chimney as well as the new density values.

The system is solved by using the Bernoulli's principle. Taking the reference pressure on the lower boundary of the cell P_0 and according to the hydrostatic gradient, the pressure due to stack effect P_i only at height z is:

$$P_i = P_{o,i} - \rho_i g z \quad (7)$$

$$\rho_i = \rho_0 \frac{T_0}{T_0 + T_i} \quad (8)$$

Boundaries between volumes are established in terms of ΔP to account for the interaction between adjacent volumes. This substitution is then input into the mass conservation equation in and rewritten in terms of Bernoulli:

$$\sum_{k=1}^{j} \dot{m}_{ik} = \sum_{k=1}^{j} \rho_{ik} \left[C_d S \sqrt{\frac{2\Delta P_i}{\rho_{mean}}} \right] = 0 \quad (9)$$

The model solves a system of n nonlinear equations that satisfy (1) until the convergence criterion of $1e^{-6}$ is met.

V. Results and Discussions

A. Analysis of Environmental Conditions

As stated before, the SC analyzed in this article is located in the PSA at Tabernas, Spain. The region of Tabernas, located next to Almeria is well known for the high mean solar radiation it receives throughout the year. In order to analyze the system, two sets of data were chosen from the month of January of the year 2016 (no PCM) and 2018 (with PCM). Both sets of data were taken from January 13th to January 25th. This data range was chosen due to the similarity in external temperature and relative low mean wind speed of 2.3 m/s.

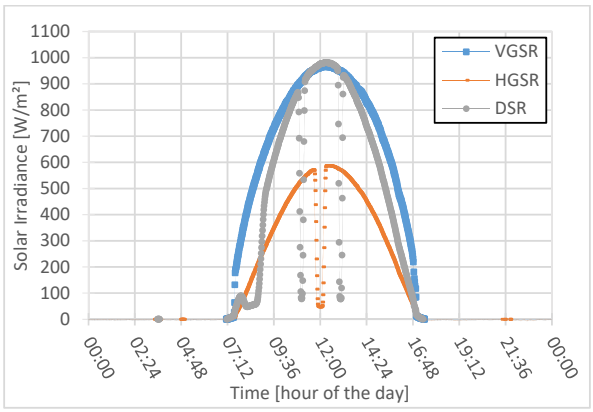

Fig. 5 Solar radiation (VGSR, HGSR and DSR) on the January 16th, 2016

Fig. 6 and 6 show the Vertical Global Solar Radiation (VGSR), Horizontal Global Solar Radiation (HGSR) and Diffuse Solar Radiation (DSR) of one particular day in the both sets of data. The information corresponds to a clear day of winter for both year samples. As mentioned by Arce et al. [10], the effects of the produced by the VGSR and the DSR can be appreciated on the surface temperature of the PCM panels, in the air temperature of the channel and the mass flow rate of the system.

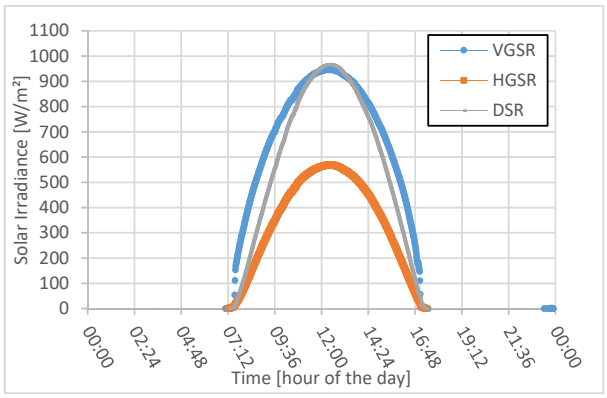

Fig. 6 Solar radiation (VGSR, HGSR and DSR) on the January 16th, 2018

In order to determine the variation in the two sets of data, a statistical analysis was carried out. In both cases, a two-sample *t* test indicated that the true difference in means was less than zero, suggesting that the environmental conditions for both sets of data are statistically equivalent. The results of the statistical analysis can be observed in TABLE .

TABLE I
Statistical Results of the Sets of Data of the SC

Variable	Standard Deviation σ	Sample mean $\bar{x}$	Probability value p-value
Wind speed SC	1.55267	2.286560	0.001479
Wind Speed ASC	1.53573	2.334002	
External temperature SC	4.17378	10.57861	< 2.2e-16
External temperature ASC	4.95966	11.17445	
Glazing temperature SC at 0.7 m	8.30379	14.21658	1.665e-09
Glazing temperature ASC at 0.7 m	10.1324	14.78302	
Glazing temperature SC at 1.7 m	7.90771	14.29569	8.794e-10
Glazing temperature ASC at 1.7 m	9.7526	14.84815	
Glazing temperature SC at 2.7 m	7.56667	14.87843	< 2.2e-16
Glazing temperature ASC at 2.7 m	9.71427	15.63444	
Glazing temperature SC at 3.15 m	7.34126	14.21181	2.301e-12
Glazing temperature ASC at 3.15 m	9.22057	14.80790	
HGSR SC	178.5357	111.8738	3.026e-15
HGSR ASC	199.3369	127.1413	
SVGSR SC	306.9163	194.2508	1.362e-11
SVGSR ASC	333.6228	216.3264	
DSR SC	298.3289	181.2074	< 2.2e-16
DSR ASC	333.2376	211.3972	

B. Outlet Temperature and External Temperature Conditions

When analyzing a system such as the SC, one of the most important variables to take into consideration is the temperature difference between inlet and outlet. In the case of this particular study, the external temperature and the inlet temperature are the same since the analysis is carried out in a stand-alone chimney. The results of three days within the sampled data are presented in Fig. 7 and Fig. 8.

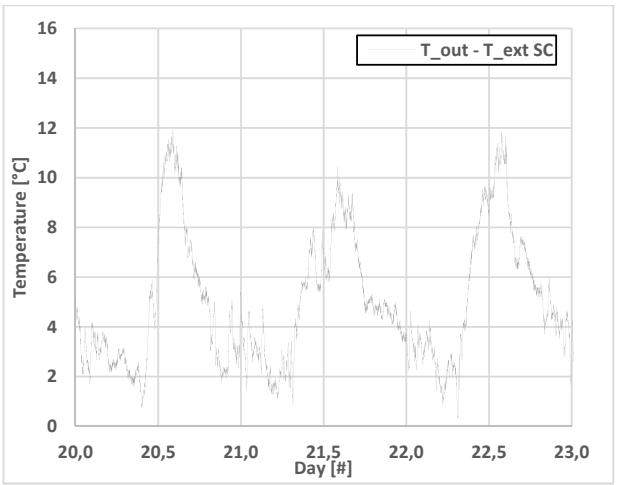

Fig. 7 Temperature difference between exterior and outlet of the data corresponding to January 20 to 23, 2016

Both results follow the temperature profile of the external temperature. In both cases, the difference between the external temperature and the outlet temperature reaches an approximate peak value of 12 °C and then drops to 2 °C. The effects of PCM can be appreciated in Fig. 8 once the external temperature begins to decrease. In comparison with the results from 2016, the temperature difference does not drop abruptly as the sun starts to set. The PCM starts to release the stored energy once the panel reaches 44 °C. In comparison, the ASC maintains a higher temperature difference for the same period. In both cases, the temperature difference is less than 5 °C after 21:00.

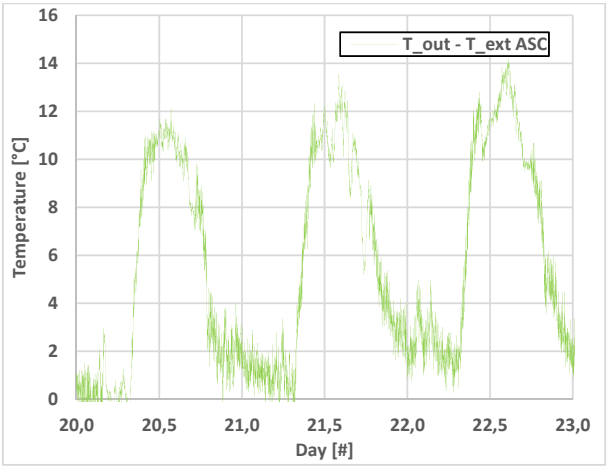

Fig. 8 Temperature difference between exterior and outlet of the data corresponding to January 20 to 23, 2018

C. PCM Panel Surface Temperature

In order to ensure the activation (energy storage and release) of the PCM panels, the surface temperature of different sections was analyzed in three different levels (Fig. 2).

The panel surface temperature across the chimney increases approximately by 5 to 6 °C every meter. The results shown in Fig. 9 correspond to the temperature registered at the central panel of the first row immediately after the inlet. The maximum temperature of those days was 20 °C, 23 °C, and 23°C respectively.

The energy storage and release can be clearly observed in the plateau of the back-surface temperature of the panel. This behavior is the result of the panel reaching its activation range (40 to 44°C). It can also be noticed that once the temperature drops to 44°C, the energy the release maintains a semi steady temperature for approximately 2.4 hours.

The mid-level panels, located at a height of 3 m, behave in a similar way as the aforementioned panel at a slightly higher temperature; however; the last row of panels does not reach 40 °C. These lower temperatures are explained by the lack of incident solar energy. Indeed, due to the geometry of the chimney, the last row of panels has no direct sunlight. This temperature drop could potentially limit the performance of the chimney.

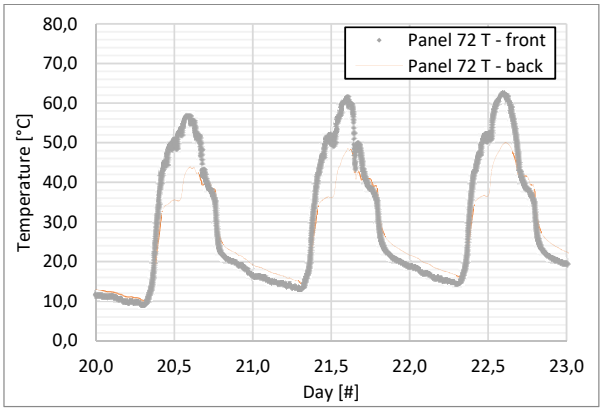

Fig. 9 Front and back surface temperature of panel 72 from January 20 to 23, 2018

D. Mass Flow Rate Results

Mass flow rate was analyzed under low wind speed conditions for both sets of data. Fig. 10 andFig. 11 are two representative samples for this type of scenario on January 16 of both years.

Overall, the mass flow rate of the ASC seems to have an increase of 11.3659 m^3/h for the sampled data with the integration of PCM panels; however, this could be due to the marginal higher temperature experienced during the 2018 data. Additionally, a slight extension of the ventilation time can be observed, yet this could be due to the same reason as stated before.

The lack of a more important ventilation rate could be due to the temperature drop at the outlet level of the chimney and should be analyzed in further studies.

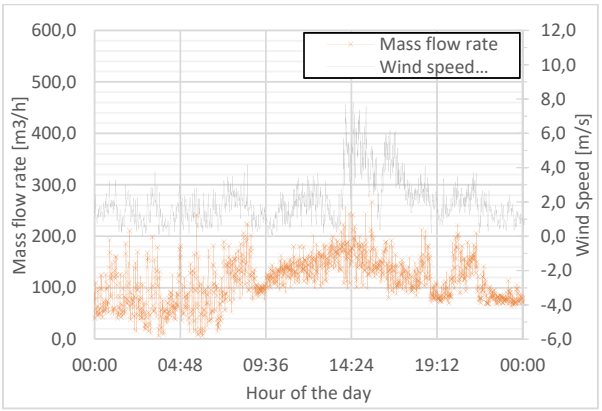

Fig. 10 Mass flow rate and wind speed data from January 16, 2016

VI. Conclusions

The performance of a stand-alone PCM integrated SC was assessed under laboratory and in situ conditions. As stated in the previous works, the laboratory results demonstrated the interest of PCM integrated SC by enhancing the mean ventilation rate when in the presence of a heat source, and a slow decrease in absence of this one. These results were obtained despite the incomplete fusion of the PCM, which

suggests that a better performance is to be expected when the complete phase change is achieved.

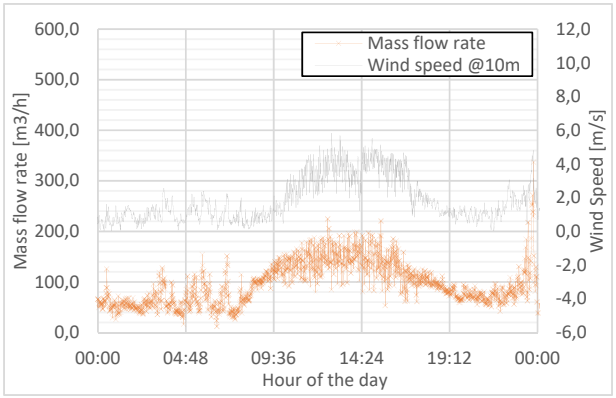

Fig. 11 Mass flow rate and wind speed data from January 16, 2018

In-situ results yielded no significant results in terms of increased mass flow rate; however, several conclusions can be made: the 15-cm concrete wall (painted black for better solar heat absorption) clearly influences the behavior of the chimney and provides a good thermal inertia to the system. This inertia is significant enough to generate similar mass flow rate results to that of the PCM integrated SC. It was observed that the concreted wall has a limited heating capability after sundown against PCM panels. Additionally, the PCM panel energy might be wasted in heating the concrete wall instead of being exploited to create a higher temperature difference in the conduit, thus reducing the impact of PCM panels. Moreover, a section of the chimney is experiencing a temperature drop, which can impact the overall ventilation rate and can particularly impact the after-sundown utilization. Furthermore, the air temperature distribution across the chimney seems to be unaffected by the addition of PCM panels; however, the results suggest that the concrete wall with PCM panels could be reduced in size or completely exchanged, thus simplifying the construction and dimensions of the system.

Finally, the results obtained since the implementation of the PCM panels will serve for the validation of the numerical model. This numerical model will be discussed in further works and will aid in the optimization of the PCM utilization.

References

[1] N. K. Bansal, R. Mathur, and M. S. Bhandari, "Solar chimney for enhanced stack ventilation," *Build. Environ.*, vol. 28, no. 3, pp. 373–377, 1993.

[2] M. M. AboulNaga and S. N. Abdrabboh, "Improving night ventilation into low-rise buildings in hot-arid climates exploring a combined wall-roof solar chimney," *Renew. Energy*, vol. 19, no. 1–2, pp. 47–54, 2000.

[3] R. Khanal and C. Lei, "A numerical investigation of buoyancy induced turbulent air flow in an inclined passive wall solar chimney for natural ventilation," *Energy Build.*, vol. 93, pp. 217–226, 2015.

[4] Z. D. Chen, P. Bandopadhayay, J. Halldorsson, C. Byrjalsen, P. Heiselberg, and Y. Li, "An experimental investigation of a solar chimney model with uniform wall heat flux," *Build. Environ.*, vol. 38, no. 7, pp. 893–906, 2003.

[5] B. Liu, X. Ma, X. Wang, C. Dang, Q. Wang, and R. Bennacer, "Experimental study of the chimney effect in a solar hybrid double wall," *Sol. Energy*, vol. 115, pp. 1–9, 2015.

[6] S. Duan, C. Jing, and E. Long, "Transient flows in displacement ventilation enhanced by solar chimney and fan," *Energy Build.*, vol. 103, pp. 124–130, 2015.

[7] M. J. Suárez-López, A. M. Blanco-Marigorta, A. J. Gutiérrez-Trashorras, J. Pistono-Favero, and E. Blanco-Marigorta, "Numerical simulation and exergetic analysis of building ventilation solar chimneys," *Energy Convers. Manag.*, vol. 96, pp. 1–11, 2015.

[8] M. Rabani, V. Kalantar, A. A. Dehghan, and A. K. Faghih, "Empirical investigation of the cooling performance of a new designed Trombe wall in combination with solar chimney and water spraying system," *Energy Build.*, vol. 102, pp. 45–57, 2015.

[9] M. H. Naraghi and S. Blanchard, "Twenty-four hour simulation of solar chimneys," *Energy Build.*, vol. 94, pp. 219–226, 2015.

[10] J. Arce, M. J. Jiménez, R. Enríquez, L. Castillo, G. Álvarez, and M. R. Heras, "Thermal performance analysis of a solar chimney , based on the experimental study of the main driving variables in a physical prototype," *Pap. Conf.*, no. October, pp. 385–395, 2015.

[11] J. C. Frutos Dordelly, M. Coillot, M. El Mankibi, R. Enriquez, M. J. Jimenez, and J. A. Landa, "Active Solar Chimney (ASC) - Numerical and experimental study of energy storage and evaporative cooling," *World Sol. Congr. Abu Dhabi*, 2017.

[12] J. Arce, J. P. Xaman, G. Alvarez, M. J. Jiménez, and M. R. Heras, "A parametric study of conjugate heat transfer of solar chimney," *Proc. ASME 3rd Int. Conf. Energy Sustain. 2009, ES2009*, vol. 1, pp. 605–612, 2009.

[13] Y. Li and S. Liu, "Numerical study on thermal behaviors of a solar chimney incorporated with PCM," *Energy Build.*, vol. 80, pp. 406–414, 2014.

[14] P. A. Mirzaei and F. Haghighat, "Modeling of phase change materials for applications in whole building simulation," *Renew. Sustain. Energy Rev.*, vol. 16, no. 7, pp. 5355–5362, 2012.

[15] D. Zhou, C. Y. Zhao, and Y. Tian, "Review on thermal energy storage with phase change materials (PCMs) in building applications," *Appl. Energy*, vol. 92, pp. 593–605, 2012.

[16] M. Kheradmand, M. Azenha, J. L. B. de Aguiar, and J. Castro-Gomes, "Experimental and numerical studies of hybrid PCM embedded in plastering mortar for enhanced thermal behaviour of buildings," *Energy*, vol. 94, pp. 250–261, 2016.